MRPL51 is a downstream target of FOXM1 in promoting the malignant behaviors of lung adenocarcinoma

WENQIAN ZHANG, LEI YU, CONG XU, TIAN TANG, JIANGUANG CAO, LEI CHEN, XINYA PANG and WEIHAO REN

Department of Thoracic Surgery, Peking University Shougang Hospital, Beijing 100144, P.R. China

Received November 16, 2022; Accepted April 21, 2023

DOI: 10.3892/ol.2023.13884

Abstract. Mitochondrial ribosome protein L51 (MRPL51) is a 39S subunit protein of the mitochondrial ribosome. Its dysregulation may be involved in non-small cell lung cancer. The present study aimed to explore MRPL51 expression in lung adenocarcinoma (LUAD) and normal lung tissues, as well as its regulatory effects on malignant LUAD behaviors. In addition, the role of forkhead box protein M1 (FOXM1) in *MRPL51* transcription was studied. Bioinformatics analysis and subsequent *in vitro* experiments, including western blotting, immunofluorescent staining, Transwell invasion assay, dual-luciferase assay and chromatin immunoprecipitation quantitative PCR were conducted. The results demonstrated that MRPL51 expression was upregulated at both the mRNA and protein levels in LUAD tissues compared with normal lung tissues. Gene Set Enrichment Analysis demonstrated that LUAD tissues with higher MRPL51 expression also had higher expression levels of genes enriched in multiple gene sets, including 'DNA_REPAIR', 'UNFOLDED_PROTEIN_RESPONSE', 'MYC_TARGETS_V1', 'OXIDATIVE_PHOSPHORYLATION', 'MTORC1_SIGNALING', 'REACTIVE_OXYGEN_SPECIES_PATHWAY', 'MYC_TARGETS_V2','E2F_TARGETS' and 'G2M_CHECKPOINT'. MRPL51 expression was positively correlated with 'cell cycle', 'DNA damage', 'DNA repair', epithelial-mesenchymal transition ('EMT'), 'invasion' and 'proliferation' of LUAD cells at the single-cell level. Compared to the negative control, *MRPL51* knockdown decreased N-cadherin and vimentin expression but increased E-cadherin expression in A549 and Calu-3 cells. MRPL51 knockdown suppressed cell proliferation, induced G1 phase arrest and decreased cell invasion. Patients with LUAD and higher MRPL51 expression had a significantly shorter overall survival (OS). FOXM1 could bind to the *MRPL51* gene promoter and activate its transcription. In conclusion, *MRPL51* was transcriptionally activated by FOXM1 in LUAD and contributed to the malignant behaviors of tumor cells, including EMT, cell cycle progression and invasion. High *MRPL51* expression may be a prognostic biomarker indicating poor OS.

Correspondence to: Dr Wenqian Zhang, Department of Thoracic Surgery, Peking University Shougang Hospital, 9 Jinyuanzhuang Road, Beijing 100144, P.R. China
E-mail: wenqian.zhang@hotmail.com

Key words: mitochondrial ribosome protein L51, forkhead box protein M1, lung adenocarcinoma, single-cell RNA sequencing, overall survival

Introduction

Lung adenocarcinoma (LUAD) is one of the main histological subtypes of non-small cell lung cancer (NSCLC). Mitochondria are complex biosynthetic, bioenergetic and signaling organelles. They serve fundamental roles in the physiological adaptations and stress responses such as bioenergetics, macromolecule biosynthesis, nutrient catabolism, and redox homeostasis to the cellular environment (1). Mitochondrial dysregulation is closely associated with the pathological development of LUAD (2,3).

Human mitochondrial DNA (mtDNA) encodes 13 essential subunits of the mitochondrial respiratory chain complexes, 22 mitochondrial transfer RNAs and two ribosomal RNAs (rRNAs) (4). The 13 protein components are synthesized by mitochondrial ribosomes (5). Human mitochondrial ribosomes comprise three rRNA molecules and ~80 interconnected mitochondrial ribosomal proteins (MRPs) encoded by nuclear DNA (6). Dysregulation of MRPs is involved in cancer development and it may be a potential cancer biomarker (7). For example, *MRPL42* gene expression can be activated by the transcription factor YY1 via promoter binding in LUAD (8). Knockdown of MRPL42 could markedly suppress proliferation, induce cell cycle arrest and reduce migration and invasion of LUAD cells *in vitro* (8). *MRPL52* upregulation is induced by hypoxia-inducible factor-1 in human breast cancer (9). Upregulation of MRPL52 is associated with aggressive clinicopathological features (such as higher histological grade, lymph node metastasis, and increased tumor size), and contributes to malignant behaviors, including epithelial-mesenchymal transition (EMT), migration and invasion of breast cancer cells (9). A recent bioinformatics study analyzed the shared dysregulated genes of musculoskeletal aging and NSCLC, and revealed that *MRPL51* is among the shared genes (10). Therefore, it is necessary to explore how MRPL51 regulates the malignant behaviors of LUAD.

Forkhead box M1 (FOXM1) is a member of the conserved forkhead box transcription factor family. Forkhead box transcription factors have a conserved winged-helix DNA-binding domain that recognizes and binds to the canonical forkhead motif RYAAAYA (11). FOXM1 upregulation promotes the progression of LUAD by enhancing cell proliferation, invasion, metastasis and resistance to gefitinib by transcriptionally activating a series of downstream target genes (12-15).

The present study aimed to explore the expression levels of *MRPL51* in normal lung tissues compared with LUAD tissues, its association with the malignant tumor behaviors of LUAD and the potential regulatory effect of FOXM1 on its aberrant upregulation.

Materials and methods

Retrieval of data from the Genotype-Tissue Expression (GTEx) project database and The Cancer Genome Atlas (TCGA). Retrieval of data from TCGA (16) and GTEx (17) was performed using the University of California, Santa Cruz (UCSC) Xena platform (https://xenabrowser.net/datapages/?cohort=TCGA%20TARGET%20GTEx&removeHub=https%3A%2F%2Fxena.treehouse.gi.ucsc.edu%3A443) (18). RNA sequencing (RNA-seq) data presented as $\log_2$(transcript per million +0.001) values were used and compared. Survival data, including progression-free interval (PFI; restricted to 56 months, the longest time without late-stage cross-over) and overall survival (OS) data, were obtained for primary LUAD cases in TCGA (n=472 with PFI data and n=510 with OS data) for Kaplan-Meier survival analysis. Median gene expression was used for the low and high *MRPL51* expression cut-off.

MRPL51 protein expression data in the Human Protein Atlas (HPA). MRPL51 expression at the protein level in normal lung and LUAD tissues was examined using immunohistochemistry (IHC) images deposited in HPA (19,20).

Cell culture and treatment. The A549 and Calu-3 human LUAD cell lines were obtained from the Cell Resource Center, Peking Union Medical College [which is the headquarters of the National Science & Technology Infrastructure-National BioMedical Cell Line Resource (NSTI-BMCR)]. 293T cells were obtained from Procell Life Science & Technology Co., Ltd. In brief, all these cell lines were cultured in Dulbecco's Modified Eagle Medium (DMEM; Gibco; Thermo Fisher Scientific, Inc.), supplemented with 10% fetal bovine serum (FBS; Gibco; Thermo Fisher Scientific, Inc.) and 1% penicillin-streptomycin solution (100 U/ml penicillin and 100 μg/ml streptomycin). Cells were cultured in a humidified environment with 5% CO_2 at 37˚C.

Lentiviral *MRPL51* and *FOXM1* short hairpin (sh)RNAs were produced using the pLKO.1-puro vector (Addgene, Inc.). The following shRNA sequences were used: shMRPL51#1, 5'-CGCATCCGCTATCTCTACAAA-3'; shMRPL51#2, 5'-GTTCGGAGTGTATGACAACAT-3'; shMRPL51#3, 5'-CTTAATAAACGCATCCGCTAT-3'; shFOXM1#1, 5'-GCCCAACAGGAGTCTAATCAA-3'; shFOXM1#2, 5'-GCACTATCAACAATAGCCTAT-3'; and shFOXM1#3, 5'-CGCCGGAACATGACCATCAAA-3'. A scramble sequence was used as the negative control (NC): shNC, 5'-CCTAAGGTTAAGTCGCCCTCG-3'.

The lentiviruses used for infection were generated using the 2nd generation system, which included the psPAX2 packaging plasmid, the pMD2.G envelope plasmid and 293T cells. In total, 1 μg pLKO.1 shRNA plasmid, 750 ng psPAX2 packaging plasmid and 250 ng pMD2.G envelope plasmid were resuspended in 20 μl serum-free OPTI-MEM (Gibco; Thermo Fisher Scientific, Inc.). Transfection into 293T cells was performed using FuGENE 6 transfection reagent (Promega Corporation) at room temperature for 30 min, according to the manufacturer's instruction. Media from the cell culture was harvested and centrifuged at 245 x g for 5 min at 4˚C. Then, the media was filtered through a 0.45 μm filter to remove the cells.

Reverse transcription-quantitative PCR (RT-qPCR). The knockdown efficiency of lentiviral *MRPL51* and *FOXM1* shRNAs in A549 and Calu-3 cells was examined 48 h after infection (MOI=10) by RT-qPCR. Total RNAs were extracted from cells using TRIzol Reagent (Thermo Fisher Scientific, Inc.). cDNA was reversely transcribed using the High-Capacity cDNA Reverse Transcription Kit (Thermo Fisher Scientific, Inc.) according to the manufacturer's instruction. qPCR was performed using FastStart Universal SYBR Green Master Mix (Roche Diagnostics), with a 7900HT Fast Real Time PCR System (Thermo Fisher Scientific, Inc.). The following primers were used: *MRPL51* forward, 5'-GATCGTTGGAACGAGAAAAGGGC-3' and reverse, 5'-CCCTTTCCAACCTCGAAGCCAT-3'; *FOXM1* forward, 5'-TCTGCCAATGGCAAGGTCTCCT-3' and reverse, 5'-CTGGATTCGGTCGTTTCTGCTG-3'; and β-actin (*ACTB*) forward, 5'-CACCATTGGCAATGAGCGGTTC-3' and reverse, 5'-AGGTCTTTGCGGATGTCCACGT-3'. The following thermocycler conditions were used: Stage 1, 50˚C for 2 min and 95˚C for 10 min; Stage 2, 95˚C for 15 sec and 60˚C for 1 min, 40 cycles; Stage 3 (dissociation curve), 95˚C for 15 sec, 60˚C for 15 sec and 95˚C for 15 sec. Relative gene expression was calculated using the $2^{-\Delta\Delta Cq}$ method (21), and *ACTB* was used as the control gene.

Western blotting. In brief, A549 and Calu-3 cell samples were collected and lysed using RIPA lysis buffer following the manufacturer's instruction (Beyotime Institute of Biotechnology). The concentration of proteins in the supernatant was measured using a BCA kit (Beyotime Institute of Biotechnology). A total of 25 μg per lane of each sample was separated by 10% SDS-PAGE and transferred onto nitrocellulose membranes. The membranes were washed with 1X TBST (0.1% Tween-20 in 1X TBS), blocked with 1X TBST containing 5% non-fat dry milk for 1 h at room temperature, and incubated with primary antibodies at 4˚C overnight. The following primary antibodies and dilutions were used: Anti-MRPL51 (1:1,000; cat. no. PA5-58988; Thermo Fisher Scientific, Inc.), anti-E-cadherin (1:1,000; cat. no. 20874-1-AP; Proteintech Group, Inc.), anti-N-cadherin (1:1,000; cat. no. 22018-1-AP; Proteintech Group, Inc.), anti-Vimentin (1:1,000; cat. no. 10366-1-AP; Proteintech Group, Inc.), anti-FOXM1 (1:1,000; cat. no. 13147-1-AP; Proteintech Group, Inc.) and anti-β-tubulin (1:1,000; cat. no. 10094-1-AP; Proteintech Group, Inc.).

Subsequently, the membranes were washed with 1X TBST and incubated with HRP-conjugated AffiniPure goat anti-rabbit IgG (H+L) (1:5,000; cat. no. SA00001-2; Proteintech Group, Inc.) for 1 h at room temperature. The protein bands were developed using BeyoECL Star reagent (Beyotime Institute of Biotechnology) with a ChemiDoc Imaging System (Bio-Rad Laboratories, Inc.). β-tubulin served as the endogenous protein expression control.

Cell Counting Kit-8 (CCK-8) assays. CCK-8 assays were conducted using a commercial CCK-8 (Beyotime Institute of Biotechnology). In brief, A549 and Calu-3 cells with or without lentiviral-mediated MRPL51 knockdown were seeded into 96-well plates (2,000 cells/well) and allowed to attach for 2 h; 2 h after seeding was considered the 0 h time point. Cell viability was measured at 0, 24, 48 and 72 h after seeding according to the manufacturer's protocol. For this, 10 μl CCK-8 solution was added to each well and incubated in a cell incubator at 37˚C for 2 h. Absorption at 450 nm was measured using a microplate reader. All CCK-8 experiments were repeated three times with three technical repeats.

Immunofluorescent staining. In brief, A549 and Calu-3 cells ($1x10^5$ cells per well/24-well plate) grown on coverslips were fixed with 4% paraformaldehyde for 15 min at room temperature, permeabilized using 0.1% Triton X-100 in PBS for 15 min at room temperature, and blocked using 2% BSA (Beyotime Institute of Biotechnology) in PBST (0.1% Tween-20) for 30 min at room temperature. For MRPL51 and mitochondria double labeling, cells were incubated with MRPL51 rabbit polyclonal antibody (1:400; cat. no. PA5-58988; Thermo Fisher Scientific, Inc.) overnight at 4˚C. After washing, cells were incubated with Alexa Fluor® 488-conjugated anti-rabbit IgG (H+L), $F(ab')_2$ (1:2,000, cat. no. 4412, Cell Signaling Technology, Inc.) for 1 h at room temperature in the dark. Mitochondria were labeled using MitoTracker Red CMXRos (Beyotime Institute of Biotechnology) according to the manufacturer's instructions. For E-cadherin and Vimentin double labeling, cells were incubated with mouse anti-Vimentin (1:500; cat. no. 60330-1-Ig; Proteintech Group, Inc.) and rabbit anti-E-cadherin (1:250; cat. no. 20874-1-AP; Proteintech Group, Inc.) overnight at 4˚C. After washing, cells were incubated with Alexa Fluor® 488-conjugated anti-mouse and Alexa Fluor® 594-conjugated anti-rabbit (1:2,000; cat. nos. 4408 and 8889; Cell Signaling Technology, Inc.) secondary antibodies for 1 h at room temperature in the dark. The nucleus was stained with DAPI (1 μg/ml) at room temperature for 1 min. Fluorescence images were captured using an Olympus IX81 widefield fluorescence microscope (Olympus Corporation).

Gene Set Enrichment Analysis (GSEA). GSEA was performed using GSEA Desktop version 4.1.0 (https://www.gsea-msigdb.org/gsea/index.jsp). In brief, the RNA-seq data of primary LUAD cases from TCGA were separated into high and low *MRPL51* expression groups based on the median *MRPL51* expression. The difference in gene set enrichment was explored in the Human (H): hallmark gene sets within the Molecular Signatures Database (MSigDB_v2022.1; https://www.gsea-msigdb.org/gsea/msigdb/index.jsp). The following parameters were set to run GSEA: Number of permutations, 1,000; permutation type, phenotype. Only the gene sets with |normalized enrichment score (NES)|>1, nominal (NOM) P<0.05 and false discovery rate (FDR) q<0.05 were included.

Characterization of the correlation between MRPL51 expression and cellular functional states in LUAD cells at the single-cell level. MRPL51 expression at the single-cell level was characterized using the single-cell RNA-seq dataset from Kim *et al* (22) based on patient-derived xenograft (PDX) tumor cells from patients with LUAD (n=126). Subsequently, its correlation with 14 single-cell functional states of each tumor cell in this dataset, including 'stemness', 'invasion', 'metastasis', 'proliferation', 'EMT', 'angiogenesis', 'apoptosis', 'cell cycle', 'differentiation', 'DNA damage', 'DNA repair', 'hypoxia', 'inflammation' and 'quiescence', was calculated. single-cell functional state scores were obtained from CancerSEA (23). In this database, the 14 single-cell functional states were scored by individual cells. Subsequently, the correlations between gene expression and the functional states were assessed by calculating the Pearson's correlation coefficients.

Transwell assay of cell invasion. A Transwell assay of A549 and Calu-3 cells (with or without *MRPL51* knockdown) invasion was performed using a 6.5-mm Transwell chamber (8-μm pore size; Corning, Inc.) coated with Matrigel (1 mg/ml), according to a previously described protocol (24). In brief, $2x10^5$ cells in 100 μl serum-free DMEM were seeded into the top chamber. The bottom chamber was filled with 0.6 ml DMEM supplemented with 10% FBS as the attractant. The plate was further incubated at 37˚C for 24 h. Then, the invaded cells on the bottom side were visualized using a light microscope (Shenzhen Aowei Optical Instrument Co., Ltd.) and counted manually.

Cell cycle distribution. In brief, 48 h after lentiviral infections, A549 and Calu-3 cells ($1x10^6$) were collected, fixed using pre-chilled 70% ethanol (-20˚C) for 3 h, washed with FACS buffer [Multisciences (Lianke) Biotech Co., Ltd.] twice and resuspended in 500 μl DAPI (1 μg/ml), according to a previously described protocol (25). Cell cycle distribution was examined using a BD FACSCalibur flow cytometer (BD Biosciences). Cell cycle distribution was analyzed using the Watson Pragmatic algorithm with NovoExpress software (v.1.5.4; Agilent Technologies, Inc.).

Dual luciferase assays. The wild-type (WT) *MRPL51* promoter sequence (Fig. S1) and the mutant (MT) sequence were chemically synthesized using an automated DNA synthesizer [General Biology (Anhui) Co., Ltd.] and inserted into the pGL3-basic plasmid (Promega Corporation). A549 and Calu-3 cells with or without lentiviral-mediated *FOXM1* knockdown were seeded into 24-well plates ($5.0x10^4$ cells/well). After 24 h, cells were transfected with 0.5 μg of either WT or MT luciferase reporter plasmid together with the *Renilla* luciferase reporter plasmid pRL-TK (0.02 μg; Promega Corporation, using FuGENE 6 transfection reagent (Promega Corporation). After 24 h, cells were washed, lysed using the passive lysis buffer (Promega Corporation) and then subjected

to the measurement of firefly and *Renilla* luciferase activities using the Dual-Luciferase Reporter Assay System (Promega Corporation). Firefly luciferase activity was normalized to *Renilla* luciferase activity. The experiments were performed in triplicate.

Kaplan-Meier survival analysis in the Kaplan-Meier plotter. To validate the prognostic significance of *MRPL51* expression in patients with LUAD, it was meaningful to perform survival data from other databases. Therefore, validation analysis was performed using survival data collected from Kaplan-Meier plotter (http://kmplot.com/analysis/) (26), which integrated data from both TCGA and multiple datasets in the Gene Expression Omnibus (GEO). Accession numbers of the specific databases extracted from the GEO can be obtained from the supplemental materials section of the Kaplan-Meier plotter website (http://kmplot.com/analysis/index.php?p=download). To avoid analysis duplication, survival data collected from TCGA were excluded. First progression-free survival (FPS) and OS were compared between patients with the top 50% and bottom 50% of *MRPL51* expression.

Chromatin immunoprecipitation (ChIP)-qPCR assay. To understand the mechanisms of aberrant upregulation of *MRPL51* in LUAD tumor cells, the transcription factors with potential binding to the *MRPL51* promoter were investigated using available ChIP sequencing (ChIP-seq) data in the Cistrome Data Browser (CistroDB; http://cistrome.org/db/; accession no. 53260) (27). In CistroDB, no ChIP-seq data were available for LUAD cells. Therefore, 293 cells exhibiting epithelial morphology were selected for bioinformatics prediction. A ChIP assay was performed using the SimpleChIP Plus Enzymatic Chromatin IP Kit (Agarose Beads; cat. no. 9004; Cell Signaling Technology, Inc.) according to the manufacturer's protocol. In short, $4x10^6$ cells with or without FOXM1 knockdown were collected, fixed 1% with formaldehyde for 10 min at room temperature and lysed using RIPA lysis buffer following the manufacturer's instruction (Beyotime Institute of Biotechnology). Subsequently, fragmented chromatin was prepared via partial digestion with micrococcal nuclease for 20 min at 37˚C. ChIP-validated rabbit anti-FOXM1 antibody (3 μg/10^6 cells; cat. no. 13147-1-AP; Proteintech Group, Inc.) and ChIP-Grade Protein G Agarose Beads were used. Rabbit IgG (3 μg/10^6 cells, cat. no. 30000-0-AP; Proteintech Group, Inc.) served as the negative control. DNA samples were collected, purified and subsequently used as template for qPCR as described above. The primers covering the predicted FOXM1 binding site were designed as follows: Forward, 5'-TTTCAAGTCGGCGGAGAAT-3' and reverse, 5'-GAA CTCGGTATTTGTGGCTTTG-3'.

Statistical analysis. Statistical analysis was performed using GraphPad Prism (version 8.10; Dotmatics). For quantitative data, mean ± SD values were calculated based on three biological repeats of three technical repeats. For samples with assumed normal distribution by Shapiro-Wilk test, one-way ANOVA with Tukey's post hoc test was used for multiple group comparisons. For data without normality assumption, Kruskal-Wallis test with Dunn's post hoc test was performed. Pearson's correlation coefficient was calculated to estimate correlations. The log-rank test was conducted to estimate the difference between survival curves. $P<0.05$ was considered to indicate a statistically significant difference.

Results

MRPL51 is aberrantly upregulated in LUAD tissues compared with normal lung tissues. RNA-seq data were retrieved for normal lung tissues in the GTEx database and for the LUAD dataset in TCGA. *MRPL51* expression was compared among normal lung tissues (n=287), LUAD tumor-adjacent normal tissues (n=59) and LUAD tissues (n=513; Fig. 1A). The results demonstrated that *MRPL51* expression was significantly higher in LUAD tissues compared with that in either normal lung or LUAD tumor-adjacent normal tissues (Fig. 1A). IHC staining data of MRPL51 expression in normal lung and LUAD tumor sections were retrieved from HPA (28), an open and accessible database providing protein expression data in human cells, tissues and organs. MRPL51 expression in alveolar epithelial cells was nearly undetectable (Fig. 1D; left). However, medium to high MRPL51 expression was observed in LUAD tissue sections (Fig. 1D; middle and right). To visualize the distribution of MRPL51 in LUAD cells, mitochondria were double-labeled using MitoTracker and MRPL51 in A549 and Calu-3 cells (Fig. 1B and C). Florescence images confirmed the localization of MRPL51 in the mitochondria found in the cytoplasm of these two cell lines (Fig. 1B and C).

GSEA results. To explore the differences in the behaviors of LUAD tumors with high and low *MRPL51* expression, patients with primary tumors in TCGA-LUAD (n=513) were separated into two groups according to the median *MRPL51* expression. The enrichment in the hallmark gene sets was compared between the two groups. Only the gene sets with $|NES|>1$, NOM $P<0.05$ and FDR $q<0.05$ were considered significantly enriched (Fig. 2A). The detailed GSEA plots indicating the significantly enriched gene sets are shown in Fig. 2B, and the peak point of the green plot is the enrichment score (ES). The results demonstrated that the high *MRPL51* expression group exhibited significantly higher expression of genes (reflected by the positive ES values in Fig. 2A) enriched in multiple gene sets compared with the low *MRPL51* expression group, including 'DNA_REPAIR', 'UNFOLDED_PROTEIN_RESPONSE', 'MYC_TARGETS_V1', 'OXIDATIVE_PHOSPHORYLATION', 'MTORC1_SIGNALING', 'REACTIVE_OXYGEN_SPECIES_PATHWAY', 'MYC_TARGETS_V2', 'E2F_TARGETS' and 'G2M_CHECKPOINT' (Fig. 2A and B). In the plots of Fig. 2B, the location of the peaks suggested that the genes in these gene sets were upregulated in the high *MRPL51* expression group compared to the low *MRPL51* expression group.

Characterization of the association between MRPL51 expression and LUAD cellular behaviors at the single-cell level. To explore the association between *MRPL51* expression and LUAD cellular behaviors at the single-cell level, *MRPL51* expression was investigated in the single-cell RNA-seq dataset from Kim *et al* (22) based on PDX tumor cells (n=126) from patients with LUAD (Fig. 3A). A total of 14 single-cell functional state scores of every tumor cell in this dataset, including

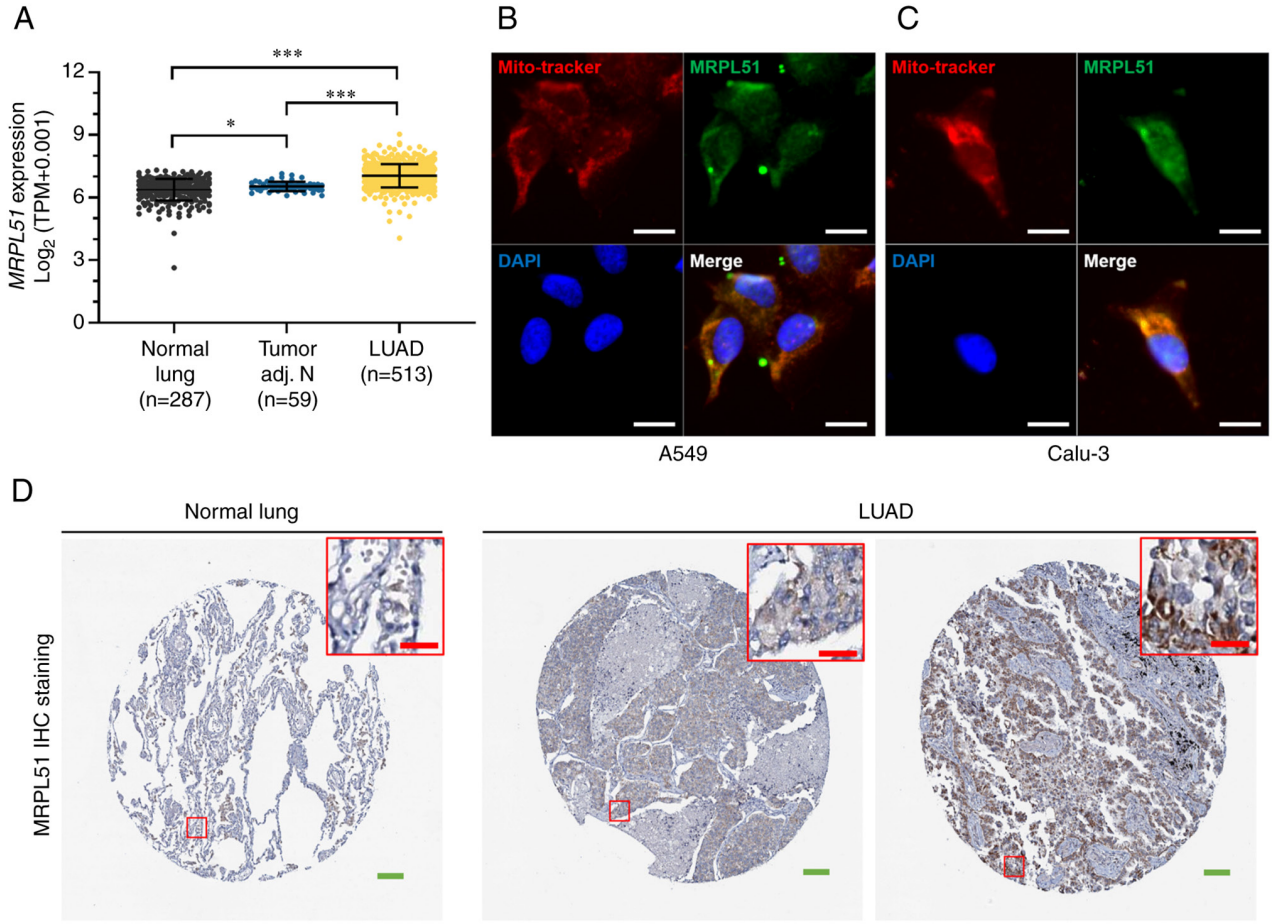

Figure 1. *MRPL51* is aberrantly upregulated in lung adenocarcinoma compared with normal lung tissues. (A) *MRPL51* expression at the mRNA level in normal lung tissues in the Genotype-Tissue Expression project database (n=287), and tumor-adjacent (n=59) and LUAD tissues (n=513) both in The Cancer Genome Atlas. Double fluorescence labeling of mitochondria (red) and MRPL51 (green) in (B) A549 and (C) Calu-3 cells. The nucleus was stained using DAPI. Scale bar, 20 μm. (D) Representative IHC staining images of MRPL51 protein expression in normal lung and LUAD tissues. Images are available from: Image/gene/data available from v21.proteinatlas.org, https://images.proteinatlas.org/39923/86665_A_2_4.jpg, https://images.proteinatlas.org/39923/85691_B_2_2.jpg and https://images.proteinatlas.org/39923/85691_B_3_3.jpg. Scale bar in green, 100 μm; scale bar in red, 25 μm. *P<0.05 and ***P<0.001. IHC, immunohistochemistry; LUAD, lung adenocarcinoma; MRPL51, mitochondrial ribosome protein L51; TPM, transcript per million. adj. N, adjacent normal.

'stemness', 'invasion', 'metastasis', 'proliferation', 'EMT', 'angiogenesis', 'apoptosis', 'cell cycle', 'differentiation', 'DNA damage', 'DNA repair', 'hypoxia', 'inflammation' and 'quiescence', were obtained from CancerSEA (23) (Fig. 3B). The correlation between *MRPL51* expression and the functional state scores was assessed by calculating Pearson's correlation coefficient. Since the cell number was relatively small (n=126), and the bioinformatics analysis only provided directions for validation studies, weak correlation (Pearson's r≥0.2) was set as the cut-off. In total, 6 out of the 14 analyzed functional states showed weak but significant correlation with *MRPL51* expression (Pearson's r≥0.2; P<0.05). In detail, *MRPL51* expression was positively correlated with 'cell cycle', 'DNA damage', 'DNA repair', 'EMT', 'invasion' and 'proliferation' of LUAD cells at the single-cell level (Fig. 3D).

Knockdown of MRPL51 increases epithelial properties, induces G1 phase arrest and weakens the invasion of LUAD tumor cells. To validate the regulatory effect of MRPL51 on cellular behaviors, lentiviral shRNA was used for *MRPL51* knockdown in A549 and Calu-3 cells (Fig. 3C and E). shMRPL51#1 and shMRPL51#2 were used for further studies due to a more optimal suppression of MRPL51 expression. *MRPL51* knockdown was associated with decreased N-cadherin and Vimentin expression, but increased E-cadherin expression in A549 and Calu-3 cells (Fig. 3E and F). A Transwell invasion assay confirmed that A549 and Calu-3 cells with *MRPL51* knockdown exhibited significantly decreased invasion (Fig. 3J-K). Flow cytometry and CCK-8 assays demonstrated that *MRPL51* knockdown induced G1 phase arrest and slowed cell proliferation (Fig. 3G-I and L-M).

MRPL51 upregulation is associated with unfavorable OS of patients with LUAD. Kaplan-Meier survival analysis was performed using PFI and OS data from TCGA-LUAD. Patients were grouped by median *MRPL51* expression. The log-rank test showed that patients with higher *MRPL51* expression (top 50%) had a similar rate of PFI [hazard ratio (HR), 1.108; 95% CI, 0.840-1.462; P=0.47] compared with the patients with lower *MRPL51* expression (bottom 50%; Fig. 4A). Patients with higher *MRPL51* expression had a significantly worse OS rate than the patients with lower *MRPL51* expression (HR, 1.462; 95% CI, 1.094-1.953; P=0.011; Fig. 4B). Using the same cut-off of *MRPL51* expression, the prognostic significance was

A

TCGA-LUAD high *MRPL51* vs. Low *MRPL51* expression (median separation)

Genesets	SIZE	ES	NES	NOM P-value	FDR q-value
HALLMARK_DNA_REPAIR	150	0.5	2.4	0	0.002
HALLMARK_UNFOLDED_PROTEIN_RESPONSE	113	0.51	2.31	0	0.001
HALLMARK_MYC_TARGETS_V1	200	0.7	2.19	0	0.002
HALLMARK_OXIDATIVE_PHOSPHORYLATION	200	0.62	2.18	0.002	0.001
HALLMARK_MTORC1_SIGNALING	200	0.55	2.1	0.002	0.002
HALLMARK_REACTIVE_OXYGEN_SPECIES_PATHWAY	49	0.54	1.94	0.016	0.011
HALLMARK_MYC_TARGETS_V2	58	0.65	1.93	0.006	0.01
HALLMARK_E2F_TARGETS	200	0.73	1.78	0.002	0.028
HALLMARK_G2M_CHECKPOINT	200	0.67	1.7	0.014	0.049

B

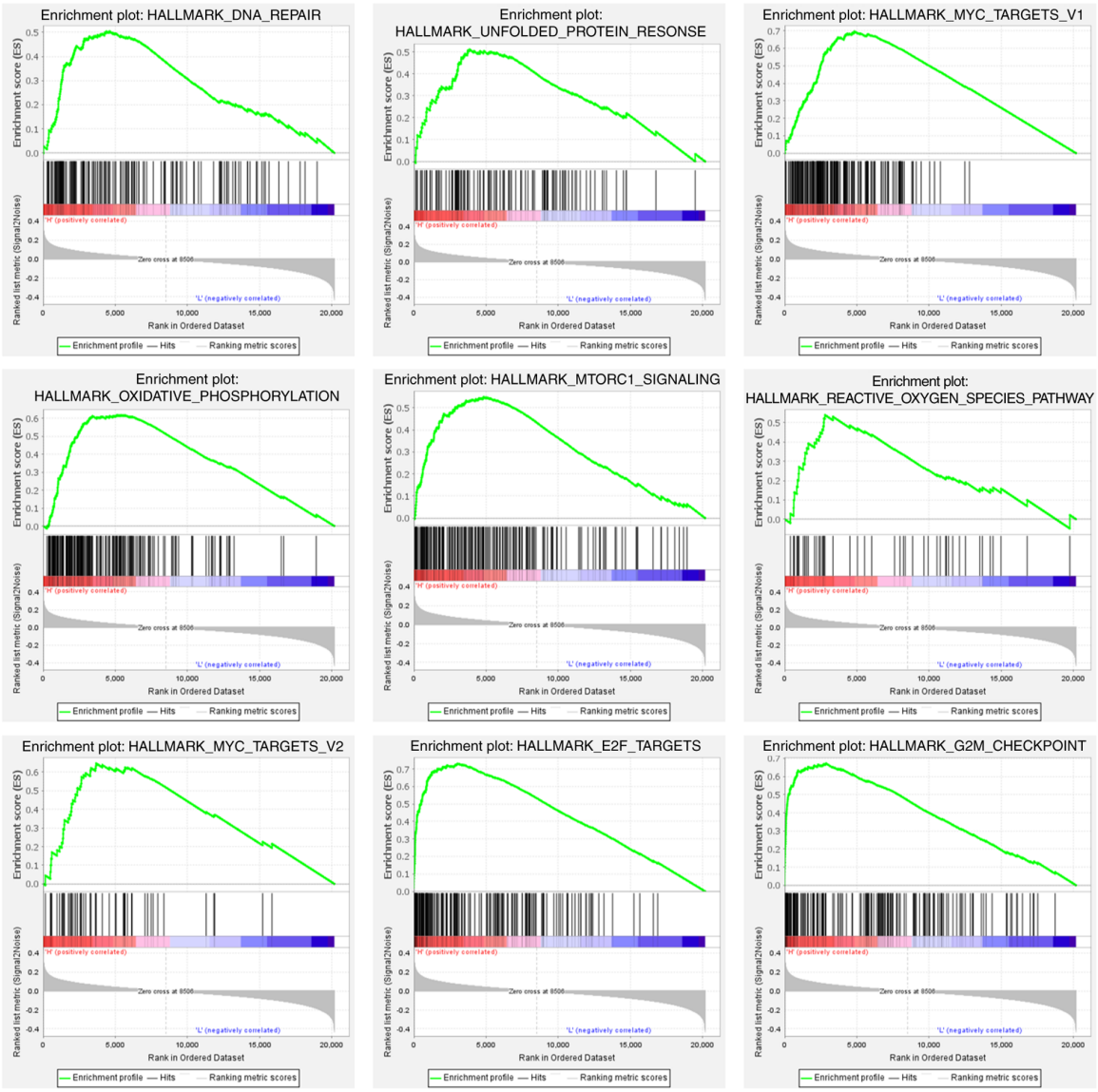

Figure 2. GSEA results. GSEA was conducted to examine the gene set enrichment of the LUAD tumor cases with high and low *MRPL51* expression in TCGA. (A) Summary table of enriched genesets and (B) the corresponding GSEA enrichment plots. Each chart's green plot corresponds to the ES. The middle red and blue bars show where the genes related to the pathways are located in the ranking. The bottom gray graph shows how the metric is distributed along the list. ES, enrichment score; FDR, false discovery rate; GSEA, Gene Set Enrichment Analysis; LUAD, lung adenocarcinoma; *MRPL51*, mitochondrial ribosome protein L51; NES, normalized enrichment score; NOM, nominal; TCGA, The Cancer Genome Atlas.

validated using data from LUAD cases in the Kaplan-Meier plotter. The log-rank test indicated that patients with higher *MRPL51* expression had a significantly worse FP probability (HR, 1.55; 95% CI, 1.12-2.14; P=0.0077; Fig. 4C) and OS rate (HR, 2.58; 95% CI, 1.97-3.38; P<0.001; Fig. 4D).

MRPL51 transcription is activated by FOXM1 in LUAD tumor cells. The transcription factors with potential binding to the *MRPL51* promoter were investigated using available ChIP-seq data in Cistrome Data Browser (CistroDB; http://cistrome.org/db/) (27). Only transcription factor genes with a regulatory

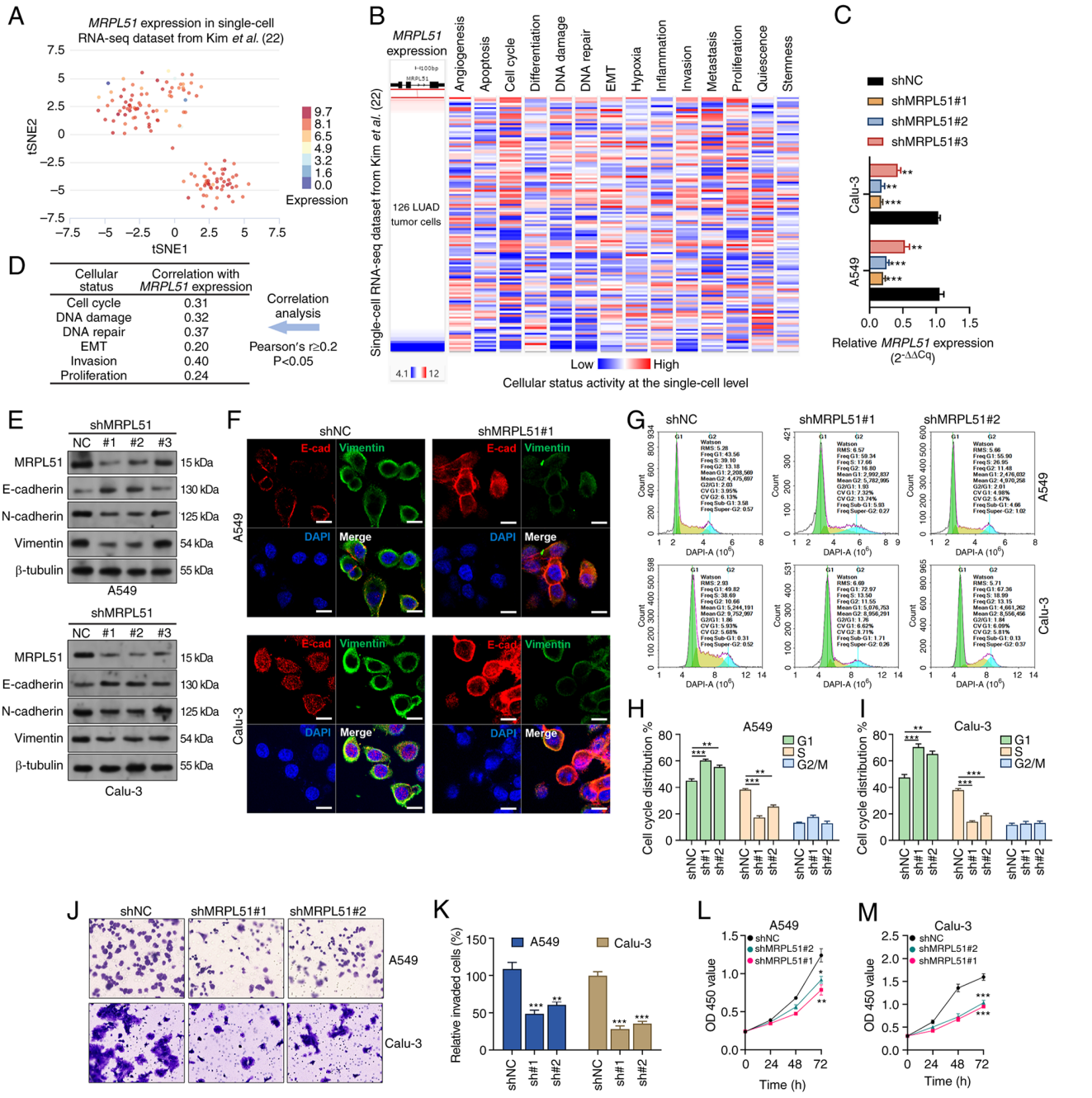

Figure 3. MRPL51 expression and LUAD cellular behaviors. (A) tSNE plots showing the distribution of cells in the single-cell dataset from Kim *et al* (22). Every point represents a single cell, and the color of the point represents the expression level of *MRPL51* in the cell. (B) Heatmap showing the correlation between *MRPL51* expression and 14 functional states at the single-cell level in the dataset from Kim *et al* (22). (C) Reverse transcription-quantitative PCR was performed to detect the expression levels of *MRPL51* in A549 and Calu-3 cells 48 h after lentivirus infection for *MRPL51* knockdown. (D) Summary table showing the functional states significantly correlated with *MRPL51* expression. (E) Western blotting was performed to detect the expression levels of MRPL51, N-cadherin, Vimentin and E-cadherin in A549 and Calu-3 cells 48 h after lentivirus infection for *MRPL51* knockdown. (F) Immunofluorescence staining was performed to visualize the expression of Vimentin and E-cadherin in A549 and Calu-3 cells 48 h after lentivirus infection for MRPL51 knockdown. Scale bar, 10 μm. (G-I) Flow cytometry (J and K) Transwell assays and (L and M) Cell Counting Kit-8 assays were performed to detect invasion, cell cycle distribution and viability of A549 and Calu-3 cells with or without *MRPL51* knockdown. Cell cycle distribution of (H) A549 and (I) Calu-3 cells, (K) Relative invaded cells (%) and the OD_{450} values of (L) A549 and (M) Calu-3 cells were quantified. In all cases, one biological group was set to 100%, while the other groups were calculated for relative expression. *P<0.05, **P<0.01 and ***P<0.001 compared with the shNC group. E-cad, E-cadherin; EMT, epithelial-mesenchymal transition; exp., expression; LUAD, lung adenocarcinoma; MRPL51, mitochondrial ribosome protein L51; NC, negative control; OD, optical density; RNA-seq, RNA sequencing; sh, short hairpin RNA; tSNE, Distributed Stochastic Neighbor Embedding.

potential >0.85 in epithelial tissues were identified as candidates, including *PATZ1, POLR2A, MYC, FOXM1, STAT1, ERG* and *MBD2* (Fig. 5A). The expression correlation between the transcription factor genes and *MRPL51* was assessed using RNA-seq data from TCGA-LUAD (Fig. 5A). Among the transcription factor genes, *FOXM1* had the strongest correlation with *MRPL51* expression (Pearson's r=0.52; Fig. 5B, data not shown for the other genes since their correlation with *MRPL51* were all <0.2). *FOXM1* expression was also significantly higher in LUAD tissues than in normal lung and

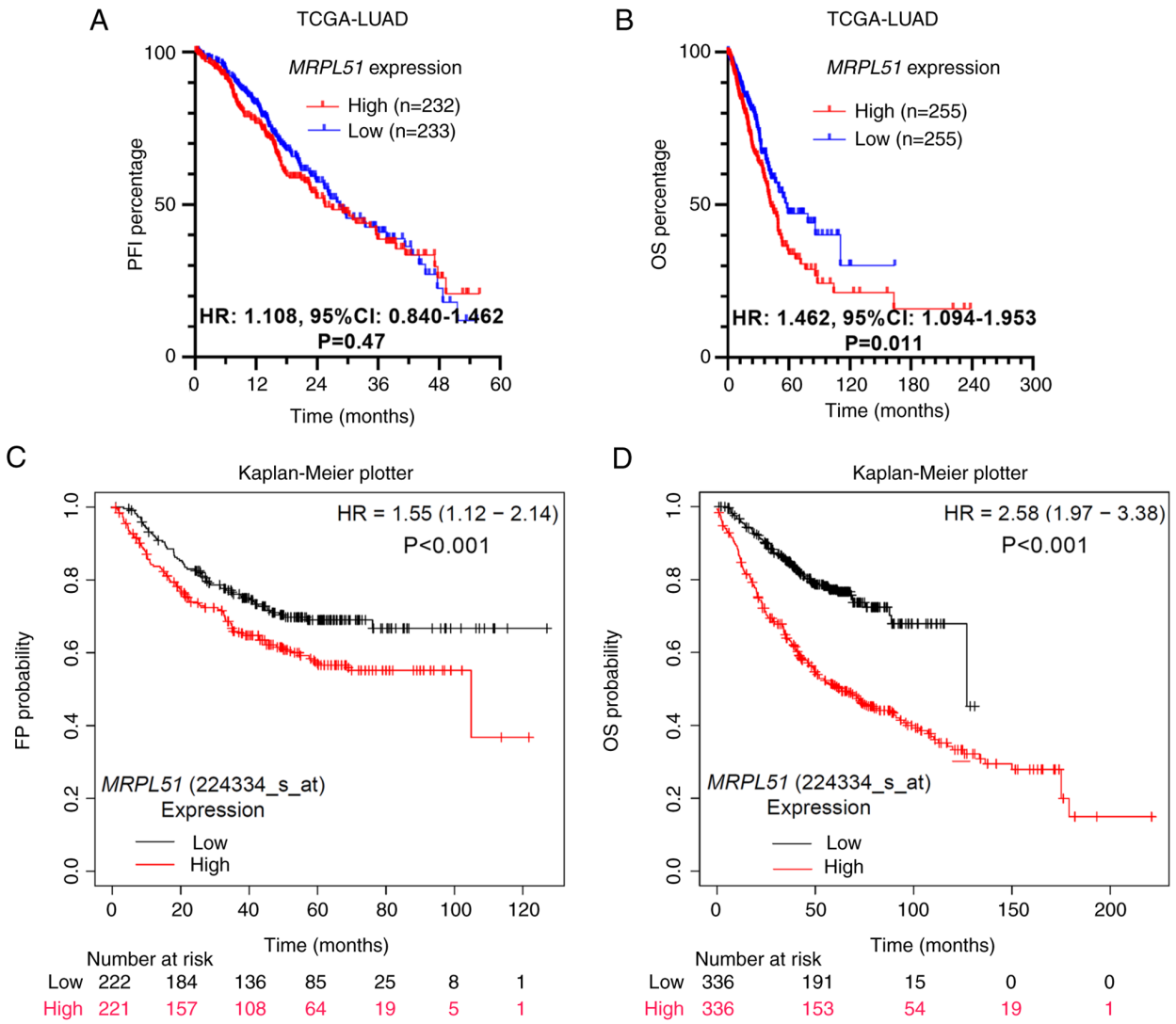

Figure 4. MRPL51 expression is associated with unfavorable OS of patients with LUAD. Kaplan-Meier survival analysis was performed using (A) PFI (months) and (B) OS time (months) from TCGA-LUAD. Patients were grouped by median *MRPL51* expression. Kaplan-Meier survival analysis was performed using (C) FPS and (D) OS data for LUAD cases from Kaplan-Meier plotter. The survival data from Kaplan-Meier plotter was collected from the Gene Expression Omnibus and TCGA. To avoid overlap, TCGA data were excluded from this analysis. Patients were grouped by median *MRPL51* expression. The log-rank test was conducted to estimate survival differences. FPS, first progression-free survival; HR, hazard ratio; LUAD, lung adenocarcinoma; MRPL51, mitochondrial ribosome protein L51; OS, overall survival; PFI, progression-free interval; TCGA, The Cancer Genome Atlas.

LUAD tumor-adjacent normal tissues (Fig. 5D). In CistroDB, no ChIP-seq data were available for LUAD cells. Therefore, 293 cells exhibiting epithelial morphology were selected for bioinformatics prediction. Using the UCSC Xena platform and the anti-FOXM1 based ChIP-seq data for 293 cells (11), it was demonstrated that the binding sites of FOXM1 in the *MRPL51* promoter (5'-ACAAATA-3') match the FOXM1 binding motif (5'-RYAAAYA-3'; Fig. 5C and E) (11). To verify the regulatory effects of FOXM1 on *MRPL51* transcription, lentiviral *FOXM1* shRNAs were generated. *FOXM1* knockdown decreased the mRNA and protein expression levels of *MRPL51* (Fig. 5F and G). shFOXM1#1 and shFOXM1#3 were used for further studies due to a more optimal suppression of FOXM1 expression. To validate the activating effect of FOXM1 on the *MRPL51* promoter, a recombinant pGL3-basic reporter plasmid carrying either wild-type (WT) [MRPL51-promoter(p)-WT] or mutant (MT) (MRPL51-p-MT, 5'-ACCCCTA-3') *MRPL51* promoter fragments was generated (Fig. 5E and I). Dual-luciferase assays confirmed that the knockdown of endogenous *FOXM1* in A549 and Calu-3 cells significantly impaired the luciferase activity of MRPL51-p-WT but had limited influence on MRPL51-p-MT (Fig. 5I). Subsequently, ChIP-qPCR was conducted using anti-FOXM1 in A549 and Calu-3 cells with or without *FOXM1* knockdown. Primers covering the predicted FOXM1 binding site were designed (blue arrows; Fig. 5E). qPCR data revealed that the *MRPL51* promoter fragments with the predicted FOXM1 binding site were enriched in the samples precipitated using anti-FOXM1 compared with IgG controls (Fig. 5H). However, *FOXM1* knockdown significantly impaired the enrichment (Fig. 5H).

Discussion

In mitochondria, MRPL51 interacts with OXA1L and participates in the biogenesis of membrane proteins and their insertion into the inner mitochondrial membrane (29). A previous study

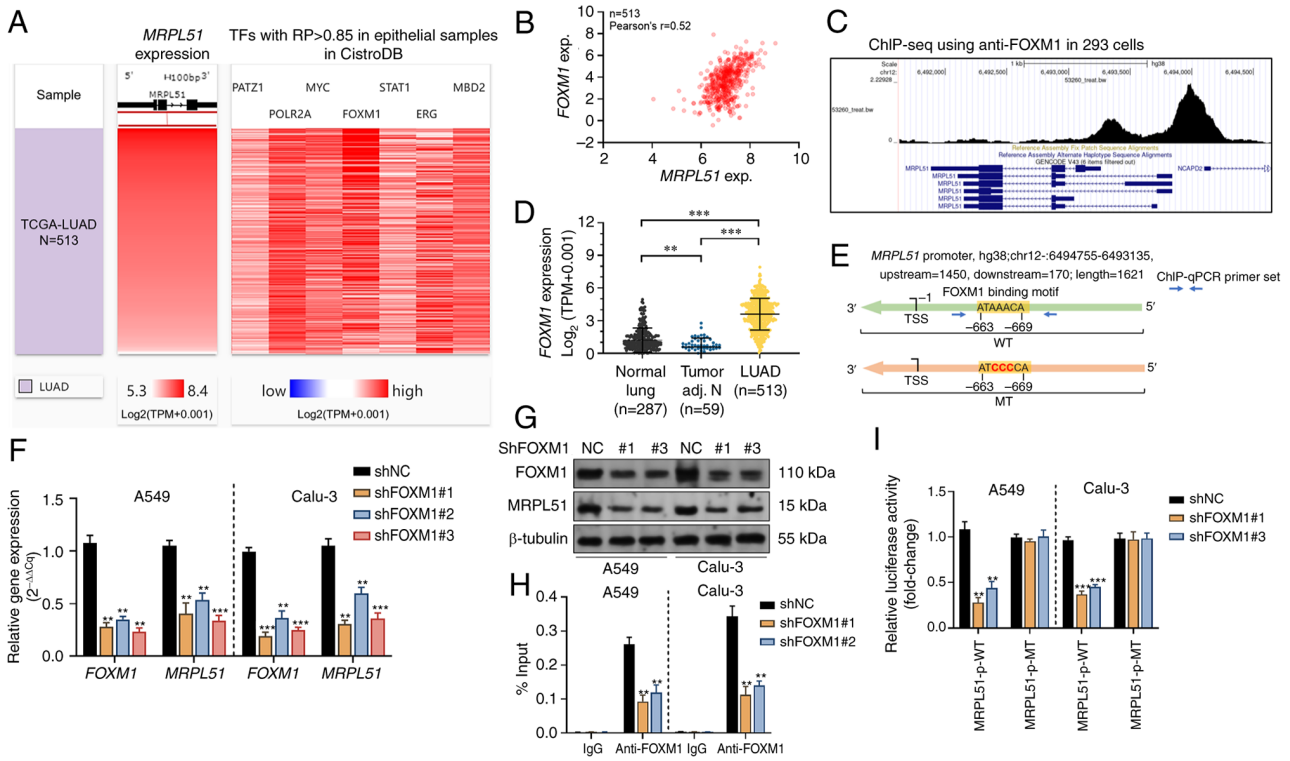

Figure 5. MRPL51 transcription is modulated by FOXM1 in LUAD tumor cells. (A) Heatmap showing the expression correlation between candidate TFs (identified using CistroDB) and *MRPL51* in primary tumor cases in TCGA-LUAD. (B) Correlation between *MRPL51* and *FOXM1* expression in TCGA-LUAD. (C) Binding site of FOXM1 on the MRPL51 promoter. Data were obtained from one previous ChIP-seq dataset (11). (D) *FOXM1* expression at the mRNA level in normal lung tissues in the Genotype-Tissue Expression project database (n=287), and tumor-adjacent (n=59) and LUAD tissues (n=513) both in TCGA. (E) Schematic charts showing the potential binding site of FOXM1 on the WT MRPL51 promoter. The MT design for the dual luciferase assay is also provided. (F) Reverse transcription-qPCR and (G) western blotting were performed to detect the expression levels of FOXM1 and MRPL51 in A549 and Calu-3 cells 48 h after lentivirus infection for *FOXM1* knockdown. (H) A ChIP assay was performed using anti-FOXM1 in cell lysates from A549 and Calu-3 cells with or without *FOXM1* knockdown. qPCR (n=3) was then performed using the primers covering the predicted FOXM1 binding site in the *MRPL51* promoter. (I) Measurement of *MRPL51* promoter activity. A549 and Calu-3 cells with or without lentiviral-mediated *FOXM1* knockdown were co-transfected with recombinant MRPL51 promoter-luciferase construct and pRL-TK plasmid. Promoter activity was examined using a dual luciferase assay kit 24 h later. **P<0.01 and ***P<0.001, compared with shNC. ChIP, chromatin immunoprecipitation; exp., expression; FOXM1, forkhead box protein M1; LUAD, lung adenocarcinoma; MRPL51, mitochondrial ribosome protein L51; MT, mutant; NC, negative control; qPCR, quantitative PCR; RP, regulatory potential; seq, sequencing; sh, short hairpin RNA; TCGA, The Cancer Genome Atlas; TFs, transcription factors; TPM, transcript per million; TSS, transcription start site; CistroDB, Cistrome Data Browser; WT, wild-type; adj.p, adjacent normal; p-, promoter-.

based on *Saccharomyces cerevisiae* revealed that MRPL51 is required for mtDNA integrity and stability, respiratory growth and mitochondrial redox homeostasis (30). However, the involvement of MRPL51 in carcinogenesis remains poorly understood. The upregulation of *MRPL51* in lung cancer was observed in a previous study (10), which may be related to gene promoter hypomethylation (31). In addition, MRPL51 is a nitric oxide (NO)-inducible gene in NSCLC cells, with >5-fold upregulation post-NO treatment (32).

In the present study, upregulation of *MRPL51* mRNA and protein expression was observed in LUAD tissues compared with normal lung tissues. GSEA based on bulk tissue RNA-seq data indicated that the LUAD cases with higher *MRPL51* expression also had upregulated genes enriched in multiple cell proliferation-related pathways, including 'G2M_CHECKPOINT', 'E2F_TARGETS' and MYC-transcriptional activity *per se* ('MYC_TARGETS_V1' and 'MYC_TARGETS_V2'). Overactive 'MTORC1_SIGNALING' is associated with enhanced EMT, motility and metastasis of lung cancer cells (33,34). The 'OXIDATIVE_PHOSPHORYLATION' and 'REACTIVE_OXYGEN_SPECIES_PATHWAY' are also the most markedly enriched pathways in tumors with increased *MRPL51* expression, according to the GSEA results of the present study. Increased generation of reactive oxygen species (ROS) in mitochondria during oxidative phosphorylation, imbalance in redox status and dysregulated redox signaling are common features during the pathological progression of LUAD (35). These alterations can lead to treatment resistance by promoting the transdifferentiation of LUAD to squamous cell carcinoma (36,37). However, ROS directly cause cell injury, including DNA damage (38,39). Cancer cells must counteract excessive oxidative damage for survival (38,39). Once the DNA is damaged, enzymatic DNA repair mechanisms are activated to maintain genomic stability and cell viability (38,39). This may explain why 'DNA_REPAIR' was identified as another significantly enriched gene set. Therefore, it was hypothesized that these enriched pathways can accumulate to lead to aggressive tumor cell behaviors.

Bulk tissue RNA-seq contains data from non-tumor cells, such as immune cells, fibroblasts and endothelial cells. To exclude the non-tumor cell signals, it was attempted to validate the association between *MRPL51* expression and the malignant behaviors of LUAD cells at the single-cell level using a previous single-cell RNA-seq dataset (22). In the present study, the

GSEA analysis demonstrated that *MRPL51* expression-related tumor cell behaviors include invasion, DNA damage, DNA repair and cell cycle progression. *In vitro* cell experiments demonstrated that *MRPL51* knockdown decreased N-cadherin and Vimentin expression, and increased E-cadherin expression in A549 and Calu-3 cells. In addition, knockdown slowed cell proliferation, induced G1 phase arrest and decreased invasion. These findings demonstrated that MRPL51 had regulatory effects on these malignant behaviors of LUAD tumor cells. This was the first study that provided direct experimental evidence indicating the tumor-promoting effects of MRPL51 in LUAD. The association between MRPL51 expression and the prognostic significance in patients with LUAD was assessed using different databases with survival data, including TCGA and Kaplan-Meier plotter. The results indicated that *MRPL51* upregulation was associated with significantly shorter OS of patients with LUAD across different databases.

Bioinformatics screening and *in vitro* assays were carried out to show that FOXM1 could bind to the *MRPL51* promoter and activate its expression. FOXM1 is aberrantly upregulated in proliferative human lung cancer cells (15,40) and regulates multiple signaling pathways by directly or indirectly elevating the transcription of target genes (41). Therefore, FOXM1 may be a potential diagnostic biomarker and treatment target in lung cancer (15). Previous studies have confirmed the association between FOXM1 upregulation and mitochondrial dysfunction, as well as their cooperative contribution to the drug resistance of lung cancer cells (42,43). Since MRPL51 regulates mtDNA integrity and stability, respiratory growth and mitochondrial redox homeostasis (30), it was hypothesized that it acts as a downstream effector of FOXM1 in promoting drug resistance of lung cancer.

The present study also has some limitations. Firstly, whether increased FOXM1 can reverse the phenotypes of downregulating MRPL51 was not explored. Future studies will aim to identify other downstream regulators of FOXM1 functionally related to MRPL51, and additional data related to the FOXM1-MRPL51 axis will be presented. Secondly, only *in vitro* experiments were conducted in the present study. Future *in vivo* studies should be conducted. In addition, since MRPL51 is related to mitochondrial functions, it is necessary to explore the links between its dysregulation and mitochondrial dysfunction in LUAD.

In conclusion, *MRPL51* is transcriptionally activated by FOXM1 in LUAD and contributes to the malignant behaviors of tumor cells, including EMT, cell cycle progression and invasion. In addition, high *MRPL51* expression may be a prognostic biomarker indicating poor OS.

Acknowledgements

Not applicable.

Funding

No funding was received.

Availability of data and materials

All data generated or analyzed during this study are included in this published article.

Authors' contributions

WZ, LY and CX conceived the study and wrote the manuscript. WZ, LY, CX, TT, JC, LC and XP collected and analyzed data. WZ, LY, CX, TT and WR interpreted data. WZ, LY and WR drafted and revised the manuscript. WZ and LY confirm the authenticity of all the raw data. All authors have read and approved the final manuscript.

Ethics approval and consent to participate

Not applicable.

Patient consent for publication

Not applicable.

Competing interests

The authors declare that they have no competing interests.

References

1. Sharma A, Ahmad S, Ahmad T, Ali S and Syed MA: Mitochondrial dynamics and mitophagy in lung disorders. Life Sci 284: 119876, 2021.
2. Karim L, Kosmider B and Bahmed K: Mitochondrial ribosomal stress in lung diseases. Am J Physiol Lung Cell Mol Physiol 322: L507-L517, 2022.
3. Cloonan SM and Choi AM: Mitochondria in lung disease. J Clin Invest 126: 809-820, 2016.
4. Ribas de Pouplana L: The mitochondrial tRNA conundrum. Nat Rev Mol Cell Biol 21: 361, 2020.
5. Hallberg BM and Larsson NG: Making proteins in the powerhouse. Cell Metab 20: 226-240, 2014.
6. Amunts A, Brown A, Toots J, Scheres SHW and Ramakrishnan V: Ribosome. The structure of the human mitochondrial ribosome. Science 348: 95-98, 2015.
7. Bao S, Wang X, Li M, Gao Z, Zheng D, Shen D and Liu L: Potential of mitochondrial ribosomal genes as cancer biomarkers demonstrated by bioinformatics results. Front Oncol 12: 835549, 2022.
8. Jiang W, Zhang C, Kang Y, Yu X, Pang P, Li G and Feng Y: MRPL42 is activated by YY1 to promote lung adenocarcinoma progression. J Cancer 12: 2403-2411, 2021.
9. Li X, Wang M, Li S, Chen Y, Wang M, Wu Z, Sun X, Yao L, Dong H, Song Y and Xu Y: HIF-1-induced mitochondrial ribosome protein L52: A mechanism for breast cancer cellular adaptation and metastatic initiation in response to hypoxia. Theranostics 11: 7337-7359, 2021.
10. Prokopidis K, Giannos P, Witard OC, Peckham D and Ispoglou T: Aberrant mitochondrial homeostasis at the crossroad of musculoskeletal ageing and non-small cell lung cancer. PLoS One 17: e0273766, 2022.
11. Sanders DA, Gormally MV, Marsico G, Beraldi D, Tannahill D and Balasubramanian S: FOXM1 binds directly to non-consensus sequences in the human genome. Genome Biol 16: 130, 2015.
12. Milewski D, Balli D, Ustiyan V, Le T, Dienemann H, Warth A, Breuhahn K, Whitsett JA, Kalinichenko VV and Kalin TV: FOXM1 activates AGR2 and causes progression of lung adenomas into invasive mucinous adenocarcinomas. PLoS Genet 13: e1007097, 2017.
13. Wei P, Zhang N, Wang Y, Li D, Wang L, Sun X, Shen C, Yang Y, Zhou X and Du X: FOXM1 promotes lung adenocarcinoma invasion and metastasis by upregulating SNAIL. Int J Biol Sci 11: 186-198, 2015.
14. Wang Y, Zhang W, Wen L, Yang H, Wen M, Yun Y, Zhao L, Zhu X, Tian L, Luo E, *et al*: FOXM1 confers resistance to gefitinib in lung adenocarcinoma via a MET/AKT-dependent positive feedback loop. Oncotarget 7: 59245-59259, 2016.
15. Li Y, Wu F, Tan Q, Guo M, Ma P, Wang X, Zhang S, Xu J, Luo P and Jin Y: The multifaceted roles of FOXM1 in pulmonary disease. Cell Commun Signal 17: 35, 2019.

16. Consortium GT: The genotype-tissue expression (GTEx) project. Nat Genet 45: 580-585, 2013.
17. Cancer Genome Atlas Research Network: Comprehensive molecular profiling of lung adenocarcinoma. Nature 511: 543-550, 2014.
18. Goldman MJ, Craft B, Hastie M, Repečka K, McDade F, Kamath A, Banerjee A, Luo Y, Rogers D, Brooks AN, *et al*: Visualizing and interpreting cancer genomics data via the Xena platform. Nat Biotechnol 38: 675-678, 2020.
19. Uhlén M, Fagerberg L, Hallström BM, Lindskog C, Oksvold P, Mardinoglu A, Sivertsson Å, Kampf C, Sjöstedt E, Asplund A, *et al*: Proteomics. Tissue-based map of the human proteome. Science 347: 1260419, 2015.
20. Uhlen M, Zhang C, Lee S, Sjöstedt E, Fagerberg L, Bidkhori G, Benfeitas R, Arif M, Liu Z, Edfors F, *et al*: A pathology atlas of the human cancer transcriptome. Science 357: eaan2507, 2017.
21. Livak KJ and Schmittgen TD: Analysis of relative gene expression data using real-time quantitative PCR and the 2(-Delta Delta C(T)) method. Methods 25: 402-408, 2001.
22. Kim KT, Lee HW, Lee HO, Kim SC, Seo YJ, Chung W, Eum HH, Nam DH, Kim J, Joo KM and Park WY: Single-cell mRNA sequencing identifies subclonal heterogeneity in anti-cancer drug responses of lung adenocarcinoma cells. Genome Biol 16: 127, 2015.
23. Yuan H, Yan M, Zhang G, Liu W, Deng C, Liao G, Xu L, Luo T, Yan H, Long Z, *et al*: CancerSEA: A cancer single-cell state atlas. Nucleic Acids Res 47: D900-D908, 2019.
24. Justus CR, Leffler N, Ruiz-Echevarria M and Yang LV: In vitro cell migration and invasion assays. J Vis Exp 1: 51046, 2014.
25. Kim KH and Sederstrom JM: Assaying cell cycle status using flow cytometry. Curr Protoc Mol Biol 111: 28.6.1-28.6.11, 2015.
26. Gyorffy B, Surowiak P, Budczies J and Lanczky A: Online survival analysis software to assess the prognostic value of biomarkers using transcriptomic data in non-small-cell lung cancer. PLoS One 8: e82241, 2013.
27. Zheng R, Wan C, Mei S, Qin Q, Wu Q, Sun H, Chen CH, Brown M, Zhang X, Meyer CA and Liu XS: Cistrome data browser: expanded datasets and new tools for gene regulatory analysis. Nucleic Acids Res 47: D729-D735, 2019.
28. Uhlen M, Oksvold P, Fagerberg L, Lundberg E, Jonasson K, Forsberg M, Zwahlen M, Kampf C, Wester K, Hober S, *et al*: Towards a knowledge-based human protein atlas. Nat Biotechnol 28: 1248-1250, 2010.
29. Haque ME, Elmore KB, Tripathy A, Koc H, Koc EC and Spremulli LL: Properties of the C-terminal tail of human mitochondrial inner membrane protein Oxa1L and its interactions with mammalian mitochondrial ribosomes. J Biol Chem 285: 28353-28362, 2010.
30. Sahu PK, Salim S, Pp M, Chauhan S and Tomar RS: Reverse genetic analysis of yeast YPR099C/MRPL51 reveals a critical role of both overlapping ORFs in respiratory growth and MRPL51 in mitochondrial DNA maintenance. FEMS Yeast Res 19: foz056, 2019.
31. Gu X, Huang X, Zhang X and Wang C: Development and validation of a DNA methylation-related classifier of circulating tumour cells to predict prognosis and to provide a therapeutic strategy in lung adenocarcinoma. Int J Biol Sci 18: 4984-5000, 2022.
32. Maiuthed A, Prakhongcheep O and Chanvorachote P: Microarray-based analysis of genes, transcription factors, and epigenetic modifications in lung cancer exposed to nitric oxide. Cancer Genomics Proteomics 17: 401-415, 2020.
33. Chen Y, Li WW, Peng P, Zhao WH, Tian YJ, Huang Y, Xia S and Chen Y: mTORC1 inhibitor RAD001 (everolimus) enhances non-small cell lung cancer cell radiosensitivity in vitro via suppressing epithelial–mesenchymal transition. Acta Pharmacol Sin 40: 1085-1094, 2019.
34. Ekman S, Wynes MW and Hirsch FR: The mTOR pathway in lung cancer and implications for therapy and biomarker analysis. J Thorac Oncol 7: 947-953, 2012.
35. Lisbôa da Motta L, Müller CB, De Bastiani MA, Behr GA, França FS, da Rocha RF, Minotto JB, Meurer RT, Fernandes MC, Roehe A, *et al*: Imbalance in redox status is associated with tumor aggressiveness and poor outcome in lung adenocarcinoma patients. J Cancer Res Clin Oncol 140: 461-470, 2014.
36. Kumari S, Badana AK, G MM, G S and Malla R: Reactive oxygen species: A key constituent in cancer survival. Biomark Insights 13: 1177271918755391, 2018.
37. Li F, Han X, Li F, Wang R, Wang H, Gao Y, Wang X, Fang Z, Zhang W, Yao S, *et al*: LKB1 inactivation elicits a redox imbalance to modulate non-small cell lung cancer plasticity and therapeutic response. Cancer Cell 27: 698-711, 2015.
38. da Silva Sergio LP, Mencalha AL, de Souza da Fonseca A and de Paoli F: DNA repair and genomic stability in lungs affected by acute injury. Biomed Pharmacother 119: 109412, 2019.
39. Guha D, Banerjee S, Mukherjee S, Dutta A and Das T: Reactive oxygen species: Friends or foes of lung cancer? In: Oxidative stress in lung diseases: Vol 2. Chakraborti S, Parinandi NL, Ghosh R, Ganguly NK and Chakraborti T (eds). Springer Singapore, Singapore, pp331-352, 2020.
40. Pabla S, Conroy JM, Nesline MK, Glenn ST, Papanicolau-Sengos A, Burgher B, Hagen J, Giamo V, Andreas J, Lenzo FL, *et al*: Proliferative potential and resistance to immune checkpoint blockade in lung cancer patients. J Immunother Cancer 7: 27, 2019.
41. Liao GB, Li XZ, Zeng S, Liu C, Yang SM, Yang L, Hu CJ and Bai JY: Regulation of the master regulator FOXM1 in cancer. Cell Commun Signal 16: 57, 2018.
42. Wang L, Liu J, Liu J, Chen X, Chang M, Li J, Zhou J, Bai C and Song Y: GLRX inhibition enhances the effects of geftinib in EGFR-TKI-resistant NSCLC cells through FoxM1 signaling pathway. J Cancer Res Clin Oncol 145: 861-872, 2019.
43. Wang K, Zhu X, Zhang K, Zhu L and Zhou F: FoxM1 inhibition enhances chemosensitivity of docetaxel-resistant A549 cells to docetaxel via activation of JNK/mitochondrial pathway. Acta Biochim Biophys Sin (Shanghai) 48: 804-809, 2016.